

Heat transport in rotating convection without Ekman layers

S. Schmitz and A. Tilgner

*Institute of Geophysics, University of Göttingen,
Friedrich-Hund-Platz 1, 37077 Göttingen, Germany*

(Dated: October 11, 2018)

Numerical simulation of rotating convection in plane layers with free slip boundaries show that the convective flows can be classified according to a quantity constructed from the Reynolds, Prandtl and Ekman numbers. Three different flow regimes appear: Laminar flow close to the onset of convection, turbulent flow in which the heat flow approaches the heat flow of non-rotating convection, and an intermediate regime in which the heat flow scales according to a power law independent of thermal diffusivity and kinematic viscosity.

PACS numbers: 47.27.te, 44.25.+f, 47.32.-y, 91.25.Za

It is a central problem for many areas of geo- and astrophysics to determine the heat flux through a rotating and convecting fluid layer. For example, the heat flux through the atmosphere governs weather and climate, the heat flux through stellar atmospheres determines stellar evolution, and the heat flux through planetary cores is essential for the generation of the magnetic fields of these bodies. A correspondingly large effort has already been spent on the problem. Buoyancy is driving the flow and can be balanced by either viscous or Coriolis forces, or the nonlinear terms in the equations of motion, or any combination of these. If the Coriolis force dominates the dynamics, a special type of boundary layer appears near solid boundaries, the Ekman layers, in which the viscous force is balanced by the Coriolis term. In addition, the flow in the bulk is organized into columnar vortices with their axes aligned with the rotation axis. If on the contrary nonlinear advection supersedes the Coriolis term, these columns are broken up and the style of flow known from non-rotating convection is approached [1, 2, 3]. There is an ongoing debate concerning the parameters at which the transition between these two flow regimes occurs [3, 4, 5], and we are still lacking reliable relations between the heat flux and the control parameters of the flow that would allow us to extrapolate data from laboratory experiments and numerical simulation to astrophysical objects.

Some recent work on rotating convection has focused on the Ekman layers. For instance, ref. [3] relates the Ekman layers to the transition mentioned above. Despite the inhibiting effect of rotation on turbulence, the heat flux in a rotating flow can exceed that of a non-rotating flow at equal Rayleigh number [6]. In ref. [7], this phenomenon is attributed to so called Ekman pumps, a term reserved for a certain flow pattern associated with Ekman boundary layers [8]. Here we investigate convection with free slip boundary conditions. This eliminates Ekman layers and one can discern which effect really depends on their presence. Free slip boundaries are realized to a good approximation in Nature, for example at the surface of the oceans or at the top of atmospheric layers.

Consider a plane layer of thickness d in the z -direction and of infinite extent in the x, y -plane. Let the layer be

filled with fluid of kinematic viscosity ν , thermal diffusivity κ , and thermal expansion coefficient α . Gravitational acceleration g is pointing in the negative z -direction and the layer is rotating with angular velocity Ω about the z -axis. The temperatures of the top and bottom boundaries are fixed at T_0 and $T_0 + \Delta T$, respectively. These two boundaries are assumed to be free slip, whereas periodic boundary conditions are applied in the x - and y -directions. The equations of evolution are made non-dimensional by using d^2/κ , d and ΔT for units of time, length, and temperature, respectively. These equations then become within the Boussinesq approximation for the dimensionless velocity $\mathbf{v}(\mathbf{r}, t)$ and temperature $T(\mathbf{r}, t)$:

$$\partial_t \mathbf{v} + (\mathbf{v} \cdot \nabla) \mathbf{v} + 2 \frac{Pr}{Ek} \hat{\mathbf{z}} \times \mathbf{v} = -\nabla p + Pr \nabla^2 \mathbf{v} + Ra Pr T \hat{\mathbf{z}} \quad (1)$$

$$\nabla \cdot \mathbf{v} = 0 \quad (2)$$

$$\partial_t T + \mathbf{v} \cdot \nabla T = \nabla^2 T \quad (3)$$

$\hat{\mathbf{z}}$ is the unit vector in z -direction and p collects the pressure and the centrifugal acceleration. The boundary conditions require that $T(z=0) = 1$, $T(z=1) = 0$, and that $v_z = \partial_z v_x = \partial_z v_y = 0$ at both $z=0$ and $z=1$. Three independent dimensionless control parameters appear: The Rayleigh number Ra , the Ekman number Ek , and the Prandtl number Pr . They are defined by:

$$Ra = \frac{g\alpha\Delta T d^3}{\kappa\nu}, \quad Ek = \frac{\nu}{\Omega d^2}, \quad Pr = \frac{\nu}{\kappa} \quad (4)$$

The Reynolds number Re and the Nusselt number Nu are an output of the simulations:

$$Re = \frac{1}{Pr} \sqrt{\frac{1}{V} \int \langle \mathbf{v}^2 \rangle dV}, \quad Nu = -\frac{1}{A} \int \langle \partial_z T \rangle dA \quad (5)$$

The angular brackets denote average over time and the integrals extend over the computational volume V for Re

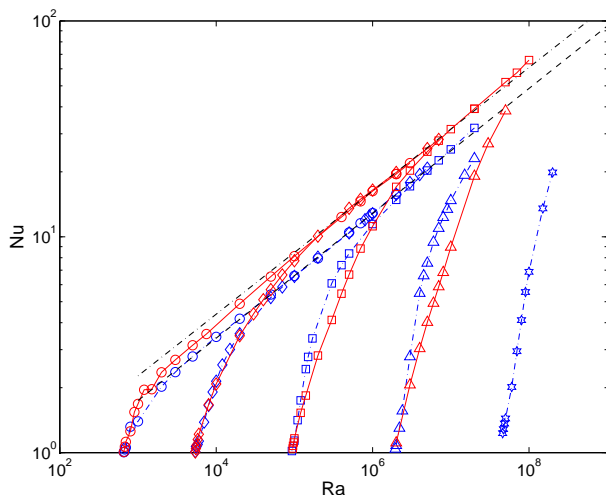


FIG. 1: Nu as a function of Ra for $Pr = 7$ (red symbols and continuous line) and 0.7 (blue symbols and dot dashed line), and $Ek = 2 \times 10^{-2}$ (diamonds), 2×10^{-3} (squares), 2×10^{-4} (triangles) and 2×10^{-5} (stars). Zero rotation is indicated by circles and the power law fits have an exponent of 0.287 .

and over the surface A of either the top or the bottom boundary for Nu .

The equations of motion were solved with the same spectral method as used in [9], except that free slip boundaries were implemented and that the Coriolis term was added and treated implicitly together with the diffusion terms. Resolutions reached up to 129 Chebychev polynomials for the discretization of the z -coordinate and 256×256 Fourier modes in the (x, y) -plane. The periodicity lengths along the x - and y - directions were always chosen to be identical. The aspect ratio, defined as the ratio of the periodicity length in the (x, y) -plane and the layer height, was fixed at 10 for simulations without rotation. In rotating convection, the typical size of flow structures varies considerably as a function of the control parameters, so that it is not useful to use a single aspect ratio. Instead, the aspect ratio was adjusted for each Ek to fit at least 8 columnar vortices along both the x - and y -directions at the onset of convection, and kept constant as Pr and Ra were varied.

Fig. 1 shows Nu as a function of Ra for various Ek and two different Pr . The case of zero rotation is included for comparison. The basic features visible in this figure are known from previous experiments and simulations [1, 3, 6, 10]. The onset of convection is delayed by rotation. After onset, Nu rises more steeply as a function of Ra than in the non-rotating case. Nu does not follow any simple power in this range of Ra . For large enough Ra , the Nu dependence asymptotes towards the dependence valid for zero rotation, which is well approximated by a power law in the investigated range of Ra .

All the different curves in fig. 1 collapse to a single curve in most of the parameter range when $(Nu-1)Ek^{1/3}$ is plotted as a function of $Re Pr Ek^{1/2}$ as shown in fig.

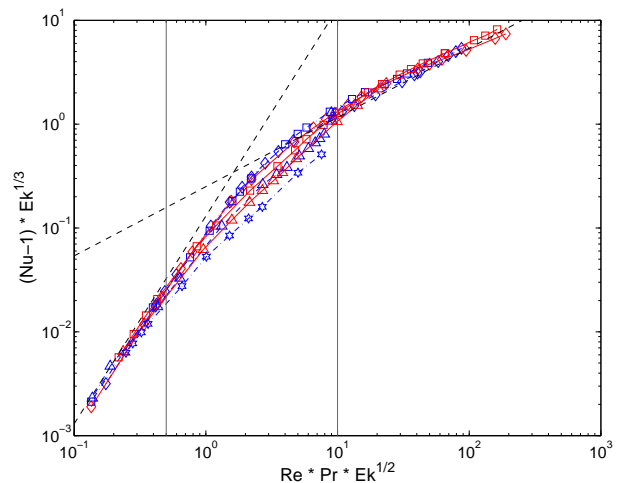


FIG. 2: $(Nu - 1)Ek^{1/3}$ as a function of $Re Pr Ek^{1/2}$ for the same data and with the same symbols as in fig. 1. The dashed lines are power laws with exponents 2 and $2/3$. The two vertical lines indicate the interval outside of which the fit to one of the two power laws is considered satisfactory.

2. For large values of $Re Pr Ek^{1/2}$ one finds $(Nu - 1)Ek^{1/3} \propto (Re Pr Ek^{1/2})^{2/3}$ or $(Nu - 1) \propto (Re Pr)^{2/3}$. This law is independent of Ek as it should be: At any fixed Ek and Pr , the limit of large Re corresponds to the situation in which the nonlinear term dominates the Coriolis term, so that one has to recover the behavior of non-rotating convection, which is of course independent of Ek . The data for zero rotation cannot be included in fig. 2 because Ek has no finite value in this case, but $(Nu - 1) \propto (Re Pr)^{2/3}$ is also found for strictly zero rotation.

Low values of $Re Pr Ek^{1/2}$ on the other hand correspond to laminar flows near the onset of convection. Forming the dot product of eq. (1) and \mathbf{v} , integrating over the whole volume and averaging over time, one finds

$$\epsilon = (Nu - 1)Ra \quad (6)$$

where $\epsilon = \frac{1}{V} \int \langle (\partial_i v_j)(\partial_i v_j) \rangle dV$ is the adimensional average dissipation rate of kinetic energy. In a laminar flow, one expects $\epsilon \propto (Re Pr)^2 / \lambda^2$, where λ is a characteristic length scale of the flow. For $Pr > 0.676$, convection starts at a critical Rayleigh number Ra_c obeying $Ra_c \propto Ek^{-4/3}$ and forms stationary cells of size λ_c with $\lambda_c \propto Ek^{1/3}$ [11]. Eq. (6) becomes $Ek^{-2/3} Re^2 Pr^2 \propto (Nu - 1)Ra$. Close to onset, $Ra \approx Ra_c$ and therefore $(Nu - 1) \propto Re^2 Pr^2 Ek^{2/3}$. This corresponds to the left asymptote in fig. 2. Both the left asymptote and $(Nu - 1) \propto (Re Pr)^{2/3}$ become straight lines in a logarithmic plot of $(Nu - 1)Ek^{1/3}$ vs. $Re Pr Ek^{1/2}$, which explains the simple appearance of fig. 2.

Fig. 2 in summary identifies three regimes of rotating convection. Rotating laminar flow characterizes one of them, and heat transport behaves the same as in non-rotating convection in another. The transition occurs where the two asymptotes in fig. 2 cross, i.e. at

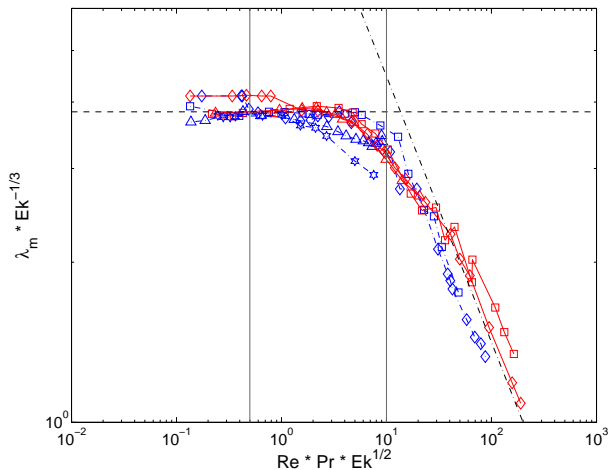


FIG. 3: $\lambda_m Ek^{-1/3}$ as a function of $Re Pr Ek^{1/2}$. The symbols have the same meaning as in fig. 1. The dashed lines indicate power laws with exponents 0 and $-1/2$.

$Re Pr Ek^{1/2} = 2$. There is a transition interval around this point of about one decade in width in which Nu is close to neither asymptote. This third regime will receive detailed attention below.

Even though Nu behaves as if there was no rotation for $Re Pr Ek^{1/2} > 10$ in fig. 2, visualizations of the flow still reveal differences. In the rotating case, the flow forms columnar vortices extending from one boundary to the other, whereas for zero rotation, plumes advected by a large scale circulation are observed. Enough visualizations of vortices in rotating convection have already appeared [1, 2, 3] so that there is no need to reproduce any here. The size of the vortices can be quantified by the method already used in [9]: Compute the time averaged advective heat transport through the plane $z = 0.5$, $\langle v_z \Theta \rangle$, with $\Theta = T - 1/2$, compute the Fourier transform of $\langle v_z \Theta \rangle$, and plot the spectrum of $\langle v_z \Theta \rangle$ as a function of wavelength λ (see [9] for detailed formulas). The median wavelength λ_m is extracted from the spectra, such that the heat advected at wavelengths smaller than λ_m equals the heat advected at larger wavelengths. The value of $\lambda_m/2$ matches the diameter of the columnar vortices identified visually in the flow field. Fig. 3 shows $\lambda_m Ek^{-1/3}$ as a function of $Re Pr Ek^{1/2}$. It is seen that λ_m stays at the onset wavelength λ_c well into the transition interval and decreases at high $Re Pr Ek^{1/2}$. This decrease follows $\lambda_m \propto (Re Pr)^{-1/2}$ at fixed Ek , which is compatible with experimental data in [12].

Near the onset of convection, the heat transport is determined by a balance between buoyancy, Coriolis and diffusive terms. For high $Re Pr Ek^{1/2}$, the Coriolis term is overwhelmed by the nonlinear term in eq. (1) so that Nu is the same as in turbulent, non-rotating convection. Diffusive processes play a role because all heat has to cross the thermal boundary layers diffusively. Let us assume as a working hypothesis that the heat flow in the intermediate regime is governed by a competi-

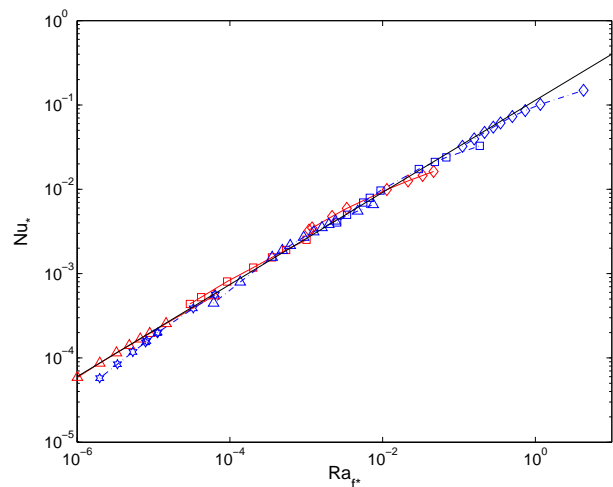


FIG. 4: Nu_* as a function of Ra_{f*} . The symbols have the same meaning as in fig. 1. This figure contains only those data points which lie in the interval marked by vertical lines in fig. 2.

tion between the nonlinear and Coriolis terms, and that the constraints imposed by rotation on the flow structure control the heat flux, not diffusion in the boundary layers. The dimensional heat flow Q must then be given by an expression independent of κ and ν . In order to check this hypothesis, it is convenient to use a control parameter independent of κ and ν . The only combination of Ra , Ek and Pr meeting this requirement is $Ra_* = Ra Ek^2 / Pr = g\alpha\Delta T / (\Omega^2 d)$. An appropriate measure of heat flux independent of κ and ν is $Nu_* = Nu Ek / Pr = Q / (\rho c_p \Delta T \Omega d)$, in which ρ stands for the density and c_p for the heat capacity.

It is useful to replace Ra_* by the flux Rayleigh number Ra_{f*} given by $Ra_{f*} = Ra_* Nu_* = (g\alpha Q) / (\rho c_p \Omega^3 d^2)$. This combination is strictly speaking a control parameter only when Neumann conditions are imposed on the temperature field, which was not the case in our simulations. However, a parameter based on Q instead of ΔT is preferable in astrophysical applications because heat fluxes are better constrained by observations than vertical temperature differences. We will therefore seek a relation between Nu_* and Ra_{f*} . Furthermore, in a flow dominated by rotation, which is necessarily nearly two dimensional, it seems plausible that heat flow through a plane $z = const.$ should be determined solely by the dynamics in that plane. Q would then be independent of the layer height d . If our working hypothesis is correct that Q is independent of κ and ν , and assuming Nu_* is given by a power law, one has to find a scaling of the form $Nu_* \propto Ra_{f*}^\beta$. If in addition Q is independent of d , one has to find $\beta = 1/2$.

Fig. 4 shows Nu_* as a function of Ra_{f*} . The figure contains only those points for which $0.5 < Re Pr Ek^{1/2} < 10$. This transition interval is small and does not corroborate any power law $Nu_* \propto Ra_{f*}^\beta$ at fixed Ek and Pr .

However, the data for different Ek and Pr collectively define an envelope which we regard to be the genuine scaling obeyed by the Nusselt number in the transition regime. The best fit to the data in fig. 4 yields

$$Nu_* = 0.11 \cdot Ra_{f*}^{0.55} \quad (7)$$

The exponent $\beta = 0.55 \pm 0.01$ is measurably different from $1/2$. There is some scatter in the points in fig. 4 around the power law (7). This scatter can be reduced by retaining data from a smaller interval of $Re Pr Ek^{1/2}$, so that the data are less affected by scalings valid in the neighboring intervals.

Ref. [13] investigates thermal convection in a rotating spherical shell. In this geometry, convection occurs mostly outside a cylinder tangent to the inner core and coaxial with the rotation axis, whereas the flow velocities are much smaller inside the tangent cylinder. Gravitational acceleration varies radially in the simulations in ref. [13] and there is a zonal flow along circles of constant latitude which has no analog in our simulations. Despite all these differences, the heat flux in the spherical geometry obeys $Nu_* = 0.077 \cdot Ra_{f*}^{5/9}$ according to ref. [13] and the best fit to a compilation of data in ref. [14] yields $Nu_* = 0.08 \cdot Ra_{f*}^{0.55}$. The exponent in (7) appears to be very robust.

It is also interesting to draw a parallel with dimensional arguments for non-rotating convection [15]. If the heat transfer is independent of the layer thickness because it is determined by boundary layer dynamics, Nu has to behave like $Nu \propto Ra^{1/3}$. This exponent is generally not observed experimentally because of the presence of a large scale circulation. The assumption that heat transport is independent of thermal diffusivity and kinematic viscosity leads without rotation to $Nu \propto (Ra Pr)^{1/2}$.

While this scaling has been found in simulations avoiding boundary layers [16] it remains elusive in any bounded geometry. In rotating convection, fig. 4 shows that a power law independent of diffusivities is a useful fit to the data, but the heat flow still depends on the layer depth.

In summary, three different regimes of convection could be identified as a function of $Re Pr Ek^{1/2}$. For small and large values of $Re Pr Ek^{1/2}$, one approaches asymptotically the scalings valid for rotating convection near onset and non-rotating convection, respectively. The cross-over occurs in a transition interval around $Re Pr Ek^{1/2} = 2$. This contradicts the naive expectation that the transition should occur when the Rossby number $Ro = Re Ek$ equals 1. Even though Re is not a control parameter, the transition criterion is useful when observations yield some information about the flow velocities in a celestial body. A case in point is the Earth's core, for which magnetic secular variations provide us with estimates of typical flow velocities around $5 \times 10^{-4} m/s$. Together with $\Omega = 7.29 \times 10^{-5} s^{-1}$ and the generally accepted material properties inside the core of $\kappa = 3 \times 10^{-6} m^2/s$ and $\nu = 5 \times 10^{-7} m^2/s$ [17], one finds $Re Pr Ek^{1/2} \approx 5$, which places the Earth's core inside the transition interval. If on the other hand the Earth's core is driven by compositional convection, a diffusivity of $7 \times 10^{-9} m^2/s$ should be used [17], leading to $Re Pr Ek^{1/2} \approx 6 \times 10^3$.

Acknowledgments

This work was supported by the Deutsche Forschungsgemeinschaft (DFG).

-
- [1] K. Julien, S. Legg, J. McWilliams, and J. Werne, *J. Fluid Mech.* **322**, 243 (1996).
 - [2] S. Stellmach and U. Hansen, *Phys. Rev. E* **70**, 056312 (2004).
 - [3] E. M. King, S. Stellmach, J. Noir, U. Hansen, and J. M. Aurnou, *Nature* **457**, 301 (2009).
 - [4] R. E. Ecke, *Phys. Rev. Lett.* **83**, 2678 (1999).
 - [5] V. M. Canuto and M. S. Dubovikov, *Phys. Rev. Lett.* **80**, 281 (1998).
 - [6] F. Zhong, R. E. Ecke, and V. Steinberg, *J. Fluid Mech.* **249**, 135 (1993).
 - [7] J.-Q. Zhong, R. J. A. M. Stevens, H. J. H. Clercx, R. Verzicco, D. Lohse, and G. Ahlers, *Phys. Rev. Lett.* **102**, 044502 (2009).
 - [8] B. Cushman-Roisin, *Introduction to Geophysical Fluid Dynamics* (Prentice Hall, Englewood Cliffs, New Jersey, 1994).
 - [9] T. Hartlep, A. Tilgner, and F. H. Busse, *Phys. Rev. Lett.* **91**, 064501 (2003).
 - [10] H. T. Rossby, *J. Fluid Mech.* **36**, 309 (1969).
 - [11] S. Chandrasekhar, *Hydrodynamic and Hydromagnetic Stability* (Oxford University Press, Oxford, 1961).
 - [12] P. Vorobieff and R. E. Ecke, *Physica D* **123**, 153 (1998).
 - [13] U. R. Christensen, *J. Fluid Mech.* **470**, 115 (2002).
 - [14] J. M. Aurnou, *Geophys. Astrophys. Fluid Dynamics* **101**, 327 (2007).
 - [15] E. A. Spiegel, *Ann. Rev. Astr. Astrophys.* **9**, 323 (1971).
 - [16] D. Lohse and F. Toschi, *Phys. Rev. Lett.* **90**, 034502 (2003).
 - [17] G. Schubert, *Treatise on Geophysics* (Elsevier, Amsterdam, 2007, volume 8, tables on pp. 140 and 191).